Reprinted from

THEORETICAL AND APPLIED MECHANICS

Volume 36

Proceedings of the 36th Japan National Congress for Applied Mechanics, 1986

Edited by Japan National Committee for Theoretical and Applied Mechanics Science Council of Japan

UNIVERSITY OF TOKYO PRESS, 1988

Numerical Simulation of Collision of Liquid Droplets

Daisuke TAKAHASHI*, Yusuke TAKEDA[2*], and Hideo TAKAMI*

**Department of Applied Physics, University of Tokyo, Tokyo, [2*]Imaging Technology Research Center, Ricoh Company Limited, Kanagawa*

A new finite difference method to compute the motion of fluid with free surfaces is proposed. This method is an improvement on the marker and cell method and by applying it the configuration of fluid regions can be visualized including free surfaces with fewer memories by the rearrangement of markers. For three-dimensional calculation of the effect of surface tension, a statistical method is introduced that saves computational time without loss of accuracy.

The computational results are shown for the splashing of a droplet, collision of a droplet with a rigid wall and collision of two droplets in axisymmetrical, two-dimensional and three-dimensional situations.

I. INTRODUCTION

In recent years, there has been increasing interest in the analysis of the motion of fluids with free surfaces. In particular, there are many interesting phenomena in the action of small drops such as ink jets or milk crowns.

The MAC (marker and cell) method[1)] and the time-dependent grid generation method[2)] are numerical methods simulating fluid motion with free surfaces. The latter has the advantage that it is easy to determine the configuration of the free surface with high accuracy. However, it is difficult to apply this method in order to calculate great deformation, merging or splitting of the fluid because it is necessary to reform the grid system.

In general, the MAC method requires a large memory and long computational time to treat the free surface. Moreover, in small-scale motion, the surface tension plays an important role in surface deformation. Therefore, few calculations have been performed for large deformation or three-dimensional cases.

We calculate the pressure at the surface by the curvature determined by the array of markers which approximate the configuration of the free surface and use fewer markers in the surface cell and rearrange them at each time step.

A smaller memory and shorter computational time are needed for the above-mentioned treatment of the surface. Consequently, we can perform three-dimensional calculations more easily. In this paper, several motions of droplets are calculated in two-dimensional, axisymmetrical and three-dimensional cases by using our improved MAC method.

II. BASIC EQUATIONS AND NUMERICAL SCHEME OF SOLUTION

The governing equations that describe the motion of the fluid are the equation of continuity and the Navier-Stokes equation. In Cartesian coordinates, they are written as follows:

$$\nabla \cdot \boldsymbol{u} = 0, \tag{1}$$

$$\frac{\partial \boldsymbol{u}}{\partial t} + (\boldsymbol{u} \cdot \nabla)\,\boldsymbol{u} = -\nabla p + \nu \Delta \boldsymbol{u}, \tag{2}$$

where $\boldsymbol{u}$ is the velocity vector, p is the pressure devided by the constant density and ν is the kinematic viscosity. By taking the divergence of the Navier-Stokes equation, we get the Poisson equation for pressure:

$$\Delta p = -\frac{\partial D}{\partial t} - \nabla \cdot ((\boldsymbol{u} \cdot \nabla)\boldsymbol{u}), \tag{3}$$

$$D = \nabla \cdot \boldsymbol{u}. \tag{4}$$

These equations are applied only in the fluid region.

In the finite-difference calculation, basic equations are approximated as follows:

$$\Delta p^n = \frac{D^n}{\Delta t} - \nabla \cdot ((\boldsymbol{u}^n \cdot \nabla)\boldsymbol{u}^n), \tag{5}$$

$$\boldsymbol{u}^{n+1} = \boldsymbol{u}^n + \Delta t(-(\boldsymbol{u}^n \cdot \nabla)\boldsymbol{u}^n - \nabla p^n + \nu \Delta \boldsymbol{u}^{n+1}), \tag{6}$$

where Δt is the interval of time differencing and the index n denotes the number of the time step. The first term of the right-hand side of Eq.(5) is put in order to set $D^{n+1} = 0$.

For space differencing, all derivatives are approximated in the form of central differencing.

On the free surface, the surface boundary conditions are as follows:

$$\sigma_{ij} n_j = 0, \tag{7}$$

$$\sigma_{ij} = -p'\,\delta_{ij} + \nu\left(\frac{\partial u_j}{\partial x_i} + \frac{\partial u_i}{\partial x_j}\right), \tag{8}$$

$$p' = p + \gamma\left(\frac{1}{R_1} + \frac{1}{R_2}\right), \tag{9}$$

where γ is surface tension and R_1 and R_2 are the principal radii of curvature of the free surface which are positive when the center of curvature exists inside the fluid region and negative when it is outside the fluid region. As it is difficult to apply all the above conditions in the finite-difference calculation, we only take account of the surface tension effect, the second term of the right-hand side of Eq. (9). The surface pressure is equal to $\gamma(1/R_1 + 1/R_2)$ and the velocity is extrapolated from the velocity inside the fluid region.

III. ALGORITHM OF CALCULATION

Using the basic equations, we simulate the fluid motion with the following algorithm (for simplicity, the situation is assumed to be two-dimensional). For example, the fluid region, the vacuum region and the wall are arranged as in Fig. 1a. The circular fluid region has downward velocity due to the gravity effect. We first make a regular mesh for the whole region (Fig. 1b). A unit of mesh is called a "cell." The physical quantity of each cell is represented at its center. To approximate the fluid region, markers are placed as in Fig. 1c and they are assumed to move with the velocity of the fluid. It is important to place markers finely enough on the surface because the configuration of the surface is essential to deter-

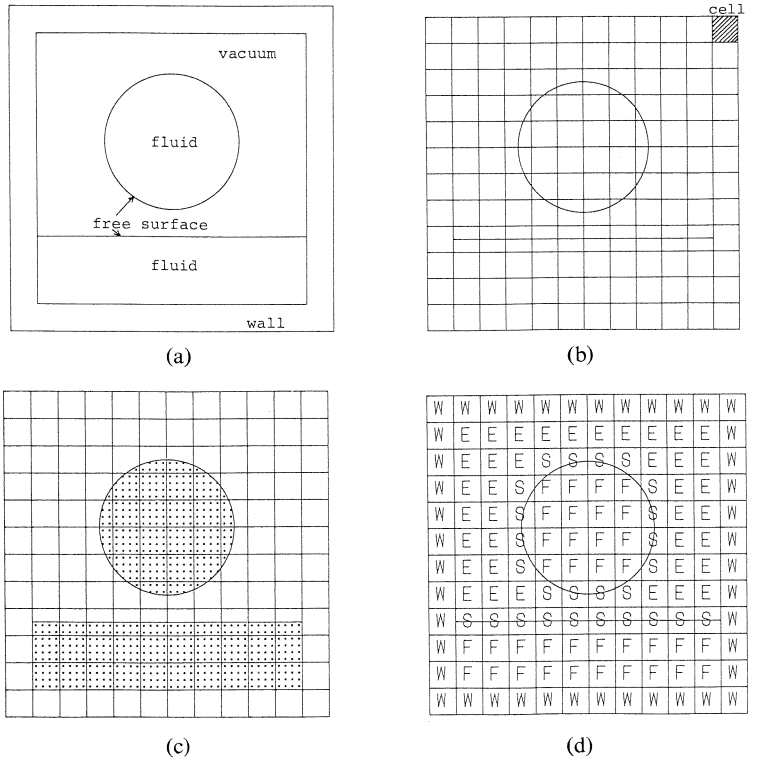

Fig. 1. Concept of MAC method.

mine the motion of the fluid. Then each cell is classified as empty (E), full (F), surface (S) and wall (W) cell. The rule of classification is as follows:

1) a cell in the wall region is a W cell;
2) a cell in which no marker exists is an E cell;
3) a cell in which some markers exist and which is adjacent to an E cell is an S cell;
4) other cells are F cells; and
5) some S cells not adjacent to F cells are renamed E cells.

An example of classification is shown in Fig. 1d. This classification roughly shows the configuration of the fluid region and each kind of cells is treated differently in the computation. The basic Eqs. (5) and (6) are applied to F cells and boundary conditions to S cells. The slip conditions of walls are applied to W cells adjacent to F cells. No equations and no conditions are applied to E cells because no fluid exists in them.

Finally, the procedure of computation is as follows:

0) At the n-th time step, markers are placed as they approximate the configuration of the fluid region and the values of velocity are given to F cells.
1) The principal radii of curvature are calculated from the positions of markers belonging to S cells and the value of pressure of S cells is calculated. The values of velocity are extrapolated from those of nearby F cells.
2) Using Eq. (5), the values of pressure of F cells at the n-th time step are calculated by an iterative method.

3) Using Eq. (6), the values of velocity of F cells at the $(n + 1)$-st time step are calculated by an iterative method.
4) Markers are moved with these velocities by a time interval Δt.
5) The configuration of the fluid region at the $(n + 1)$-st time step is determined by the positions of markers and every cell is newly classified.
6) Return to step 1.

After the calculation of large time steps using the above procedure repeatedly, large deformation, merging or splitting of the fluid region may occur and the distribution of markers may become unbalanced. Then the configuration of the fluid region cannot be clearly recognized. It is necessary to rearrange markers on the basis of the positions of markers at the previous time step. For S cells, the markers are rearranged at every time step and the number of markers in each S cell is always controlled. For F cells, the markers are necessary only when the configuration of the fluid region at the next time step is calculated and markers at the previous time step in F cells need not be memorized.

The method of calculation of curvature from the positions of markers in S cells is as follows. In two-dimensional or axisymmetrical cases, the curvature is easily calculated with the positions of three markers; one marker is selected from the S cell in question and two markers are selected from adjacent S cells. In the three-dimensional case, the recognition of the curved free surface is very difficult and a large amount of computation may be necessary. We avoid this problem using a statistical method; four markers in the S cell in question and adjacent S cells determine a unique sphere that has those markers on its surface. The average of a reciprocal of the radius of spheres determined from all combinations of four markers is taken as an approximate value of the curvature. Such treatment leads to shortened computational time.

IV. EXAMPLES OF CALCULATIONS

4.1 Splashing of a Droplet

This example shows an axisymmetrical splashing of a droplet running into a pool of the same kind of fluid and a comparison with the experimental results of Macklin and Hobbs.[3]

A droplet 2.3 mm in diameter impacts a pool 4 mm deep at a velocity of 320 cm/s. When a droplet strikes the liquid surface of the pool, the surface caves in from the impact. Subsequently the fluid near the cave concentrates and a liquid projection springs up. This calculation was performed by Amsden and Harlow[4] but they did not take account of the surface tension effect.

Numerical results are shown in Fig. 2. In this figure, velocity vectors and pressure contours are plotted on, respectively, the left- and right-hand side of the symmetry axis. Figure 3 shows the dependence of the maximum height of the liquid region on the symmetry axis on time. The maximum projection height in the experiment is about 10 mm and the calculated result is higher than the experimental one. It is suspected that this difference is caused by the difference of the boundary condition of the pool. Conditions used in this calculation are shown in Table 1.

4.2 Axisymmetrical Collision of Two Droplets

In this example, the collision of two droplets is examined by changing the diameters and velocities of droplets. Two droplets moving with the same speed in opposite directions

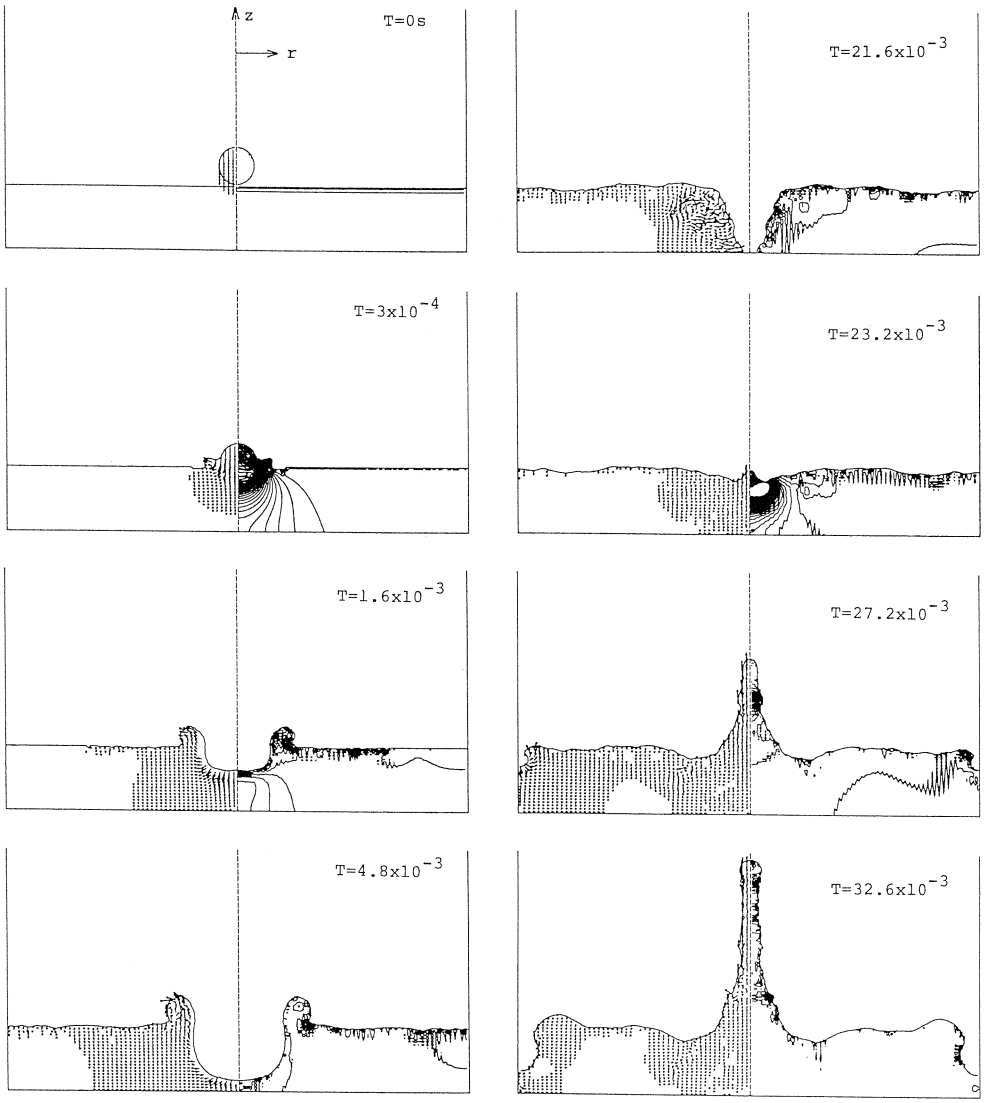

Fig. 2. Splashing of a droplet into a pool.

collide coaxially. The calculations are performed by using cylindrical coordinates and the gravity effect is neglected. Figures 4, 5 and 6 show the numerical results for surface configuration, velocity vector and pressure contours. In Fig. 4, diameters of the two droplets are both 2.0 mm and initial velocities in the z-direction are ± 50 cm/s, respectively. In Fig. 5, diameters of the droplets are 3.0 mm and 1.5 mm and initial velocities are ± 50 cm/s. In Fig. 6, diameters are 3.0 mm and 1.5 mm and initial velocities are ± 100 cm/s.

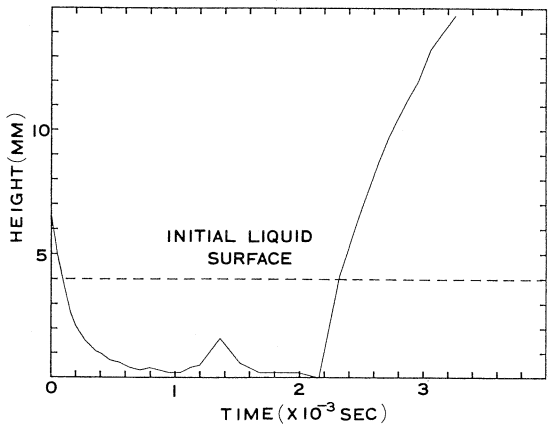

Fig. 3. Dependence of maximum height of liquid region on symmetry axis on time.

Table 1. Splashing of a droplet.

	Fig. 2
Kinematic viscosity	0.01 cm^2/s
Surface tension	75 dyn/cm
Diameter of droplet	0.23 cm
Velocity of droplet	−320 cm/s
Gravity	−1000 cm/s^2
Depth of pool	0.4 cm
Diameter of pool	3.0 cm
Mesh points	100 × 100
Mesh interval (Δr)	0.015 cm
Mesh interval (Δz)	0.01 cm
Time interval (Δt)	4×10^{-6} s

In the case of Fig. 4, two droplets merge into one body and expand in the r-direction after the collision. Then the velocity component in the z-direction increases due to the effect of surface tension, and thus the configuration of merged droplets which expanded is restored.

Figure 5 shows that merged droplets first expand and then contract as in the former case. In the case of higher velocities (Fig. 6), deformation in the r-direction is greater than in Fig. 5, but the configuration is restored as above. Conditions used in these calculations are shown in Table 2.

4.3 Collision of a Droplet with a Rigid Wall

This example shows a collision of a droplet with a rigid wall. Calculations were performed for an axisymmetrical and a two-dimensional case. For the axisymmetrical case, calculations are performed for two values of surface tension, 75 dyn/cm and 15 dyn/cm, in the cylindrical coordinates and the numerical results are shown in Fig. 7 and Fig. 8,

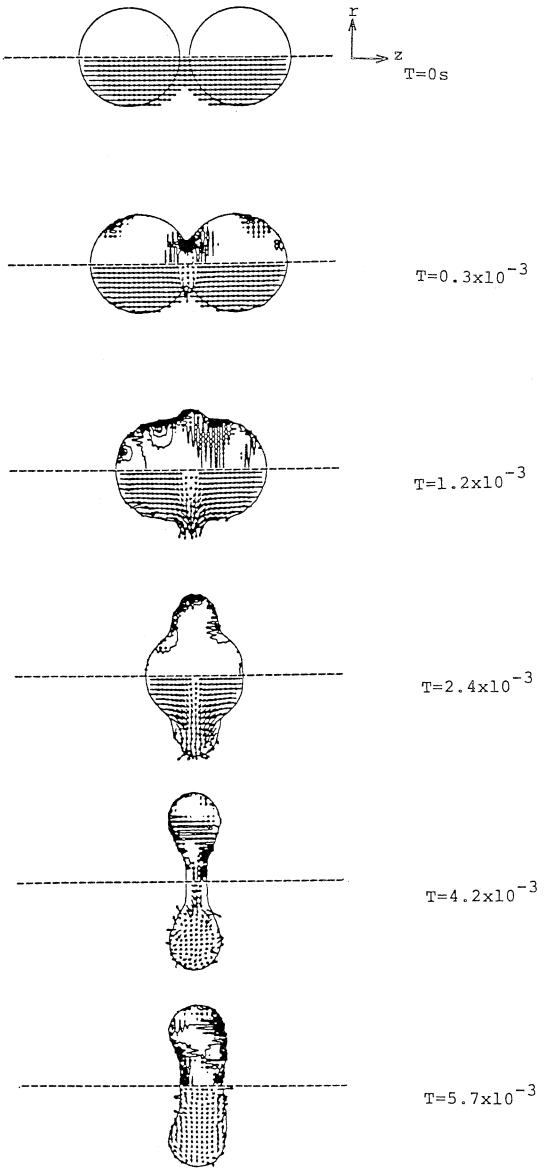

Fig. 4. Axisymmetrical collision of droplets.

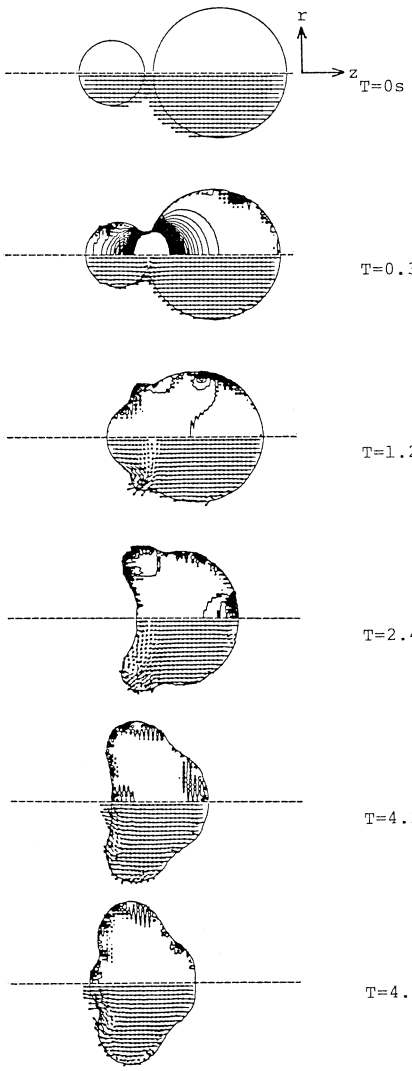

Fig. 5. Axisymmetrical collision of droplets.

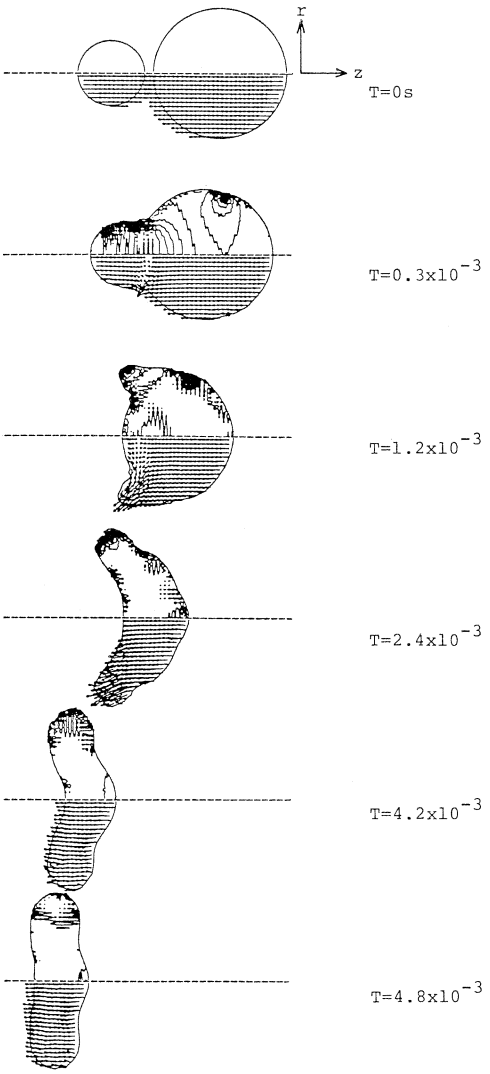

Fig. 6. Axisymmetrical collision of droplets.

Table 2. Axisymmetrical collision of two droplets.

	Fig. 4	Fig. 5	Fig. 6
Kinematic viscosity	0.01 cm^2/s	0.01 cm^2/s	0.01 cm^2/s
Surface tension	75 dyn/cm	75 dyn/cm	75 dyn/cm
Diameter of droplets	0.2 cm, 0.2 cm	0.3 cm, 0.15 cm	0.3 cm, 0.15 cm
Velocity of droplets	± 50 cm/s	± 50 cm/s	± 100 cm/s
Mesh points	$130(z) \times 80(r)$	$130(z) \times 80(r)$	$130(z) \times 80(r)$
Mesh interval (Δr)	0.005 cm	0.005 cm	0.005 cm
Mesh interval (Δz)	0.005 cm	0.005 cm	0.005 cm
Time interval (Δt)	1×10^{-6} s	1×10^{-6} s	5×10^{-7} s

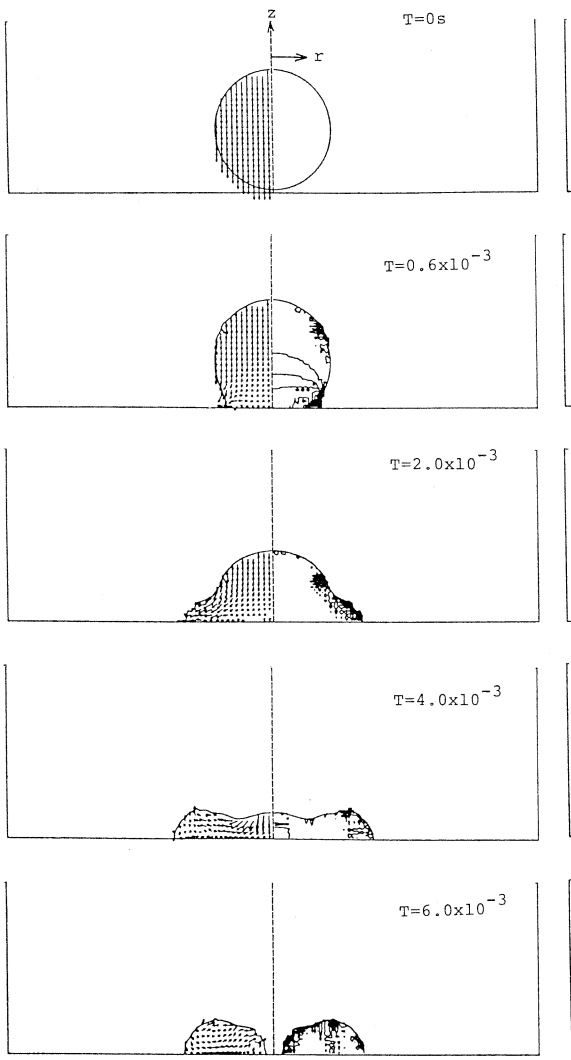

Fig. 7. Axisymmetrical collision of a droplet with a rigid wall.

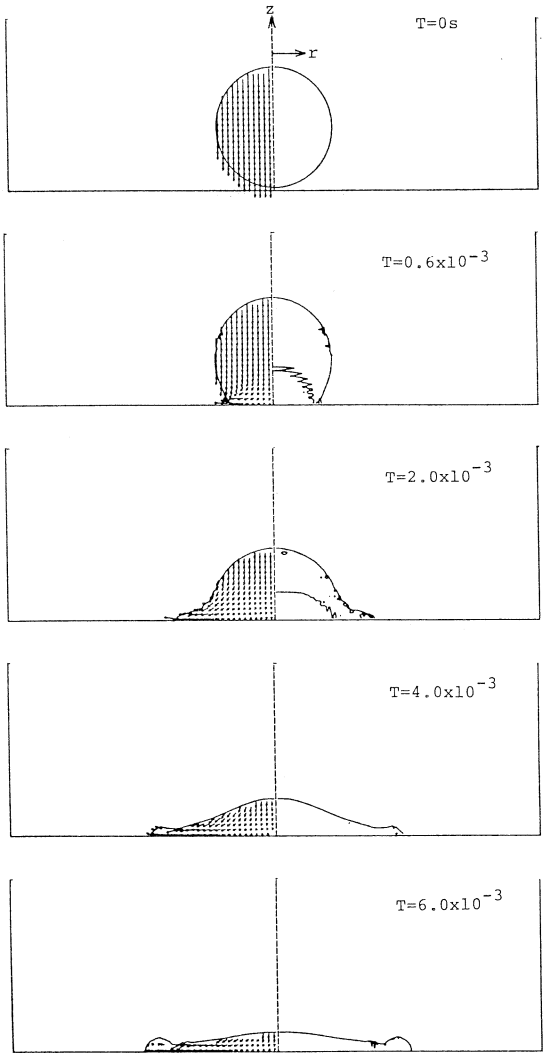

Fig. 8. Axisymmetrical collision of a droplet with a rigid wall.

Table 3. Axisymmetrical collision of a droplet with a rigid wall.

	Fig. 7	Fig. 8
Kinematic viscosity	0.01 cm^2/s	0.01 cm^2/s
Surface tension	75 dyn/cm	15 dyn/cm
Diameter of droplet	0.22 cm	0.22 cm
Velocity of droplet	−50 cm/s	−50 cm/s
Mesh size	100 × 100	100 × 100
Mesh interval (Δr)	0.005 cm	0.005 cm
Mesh interval (Δz)	0.005 cm	0.005 cm
Time interval (Δt)	1×10^{-6} s	1×10^{-6} s

respectively. Gravity is neglected, the diameter of the droplet is 2.2 mm and initial velocity is 50 cm/s in both figures. In the case of Fig. 7, the colliding droplet expands in the r-direction. Then the droplet forms a ring shape with a hole at the center due to the effect of surface tension.

On the other hand, in the case of lower surface tension (Fig. 8), the colliding droplet expands but the ring formation does not occur. Conditions used in these calculations are shown in Table 3.

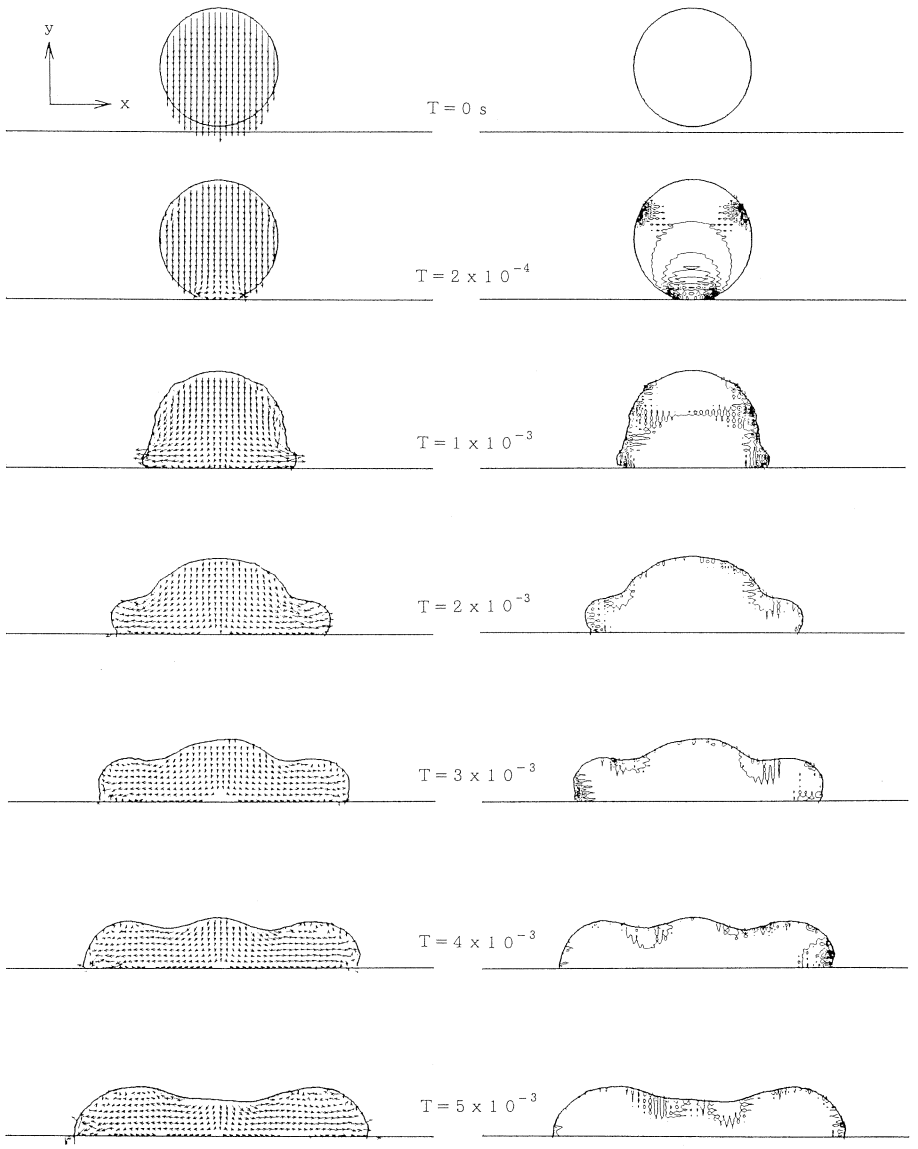

Fig. 9. Two-dimensional collision of a droplet with a rigid wall.

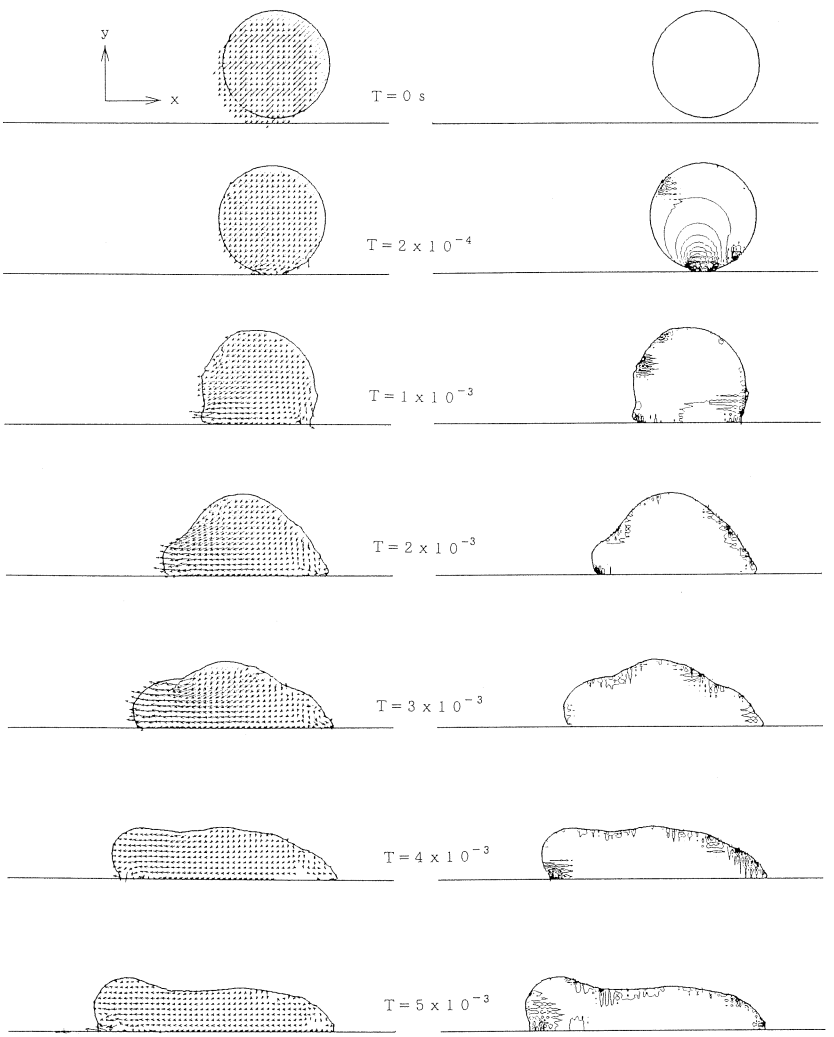

Fig. 10. Two-dimensional collision of a droplet with a rigid wall.

Table 4. Two-dimensional collision of a droplet with a rigid wall.

	Fig. 9	Fig. 10
Kinematic viscosity	0.01 cm^2/s	0.01 cm^2/s
Surface tension	75 dyn/cm	75 dyn/cm
Collision angle	90°	45°
Diameter of droplet	0.2 cm	0.2 cm
Velocity of droplet	-50 cm/s(y)	-35.4 cm/s(x, y)
Mesh points	160(x) × 60(y)	160(x) × 60(y)
Mesh interval (Δx)	0.005 cm	0.005 cm
Mesh interval (Δy)	0.005 cm	0.005 cm
Time interval (Δt)	1×10^{-6} s	1×10^{-6} s

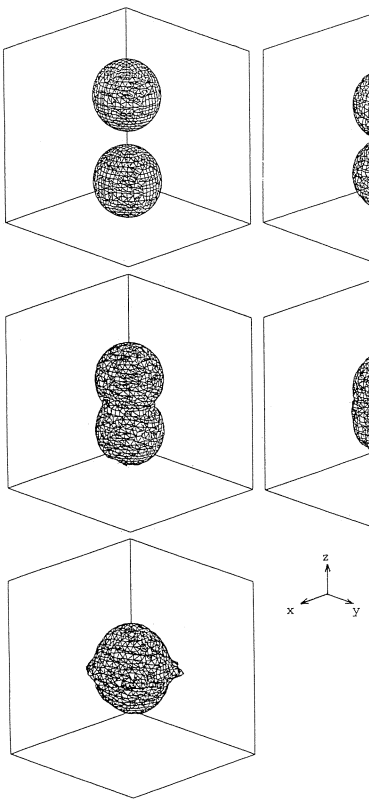

Fig. 11. Three-dimensional collision of droplets.

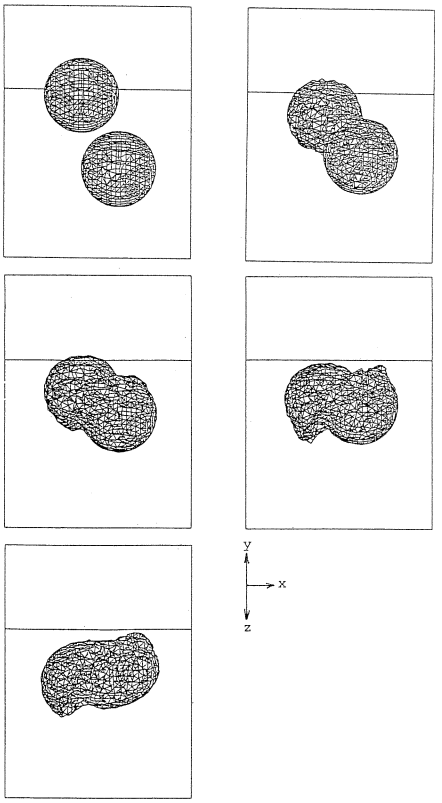

Fig. 12. Three-dimensional collision of droplets.

Table 5. Three-dimensional collision of two droplets.

	Fig. 11	Fig. 12
Kinematic viscosity	0.01 cm^2/s	0.01 cm^2/s
Surface tension	75 dyn/cm	75 dyn/cm
Diameter of droplets	2 cm, 2 cm	2 cm, 2 cm
Velocity of droplets	± 500 cm/s	± 500 cm/s
Initial position of centers of droplets (cm)	(2.5, 2.5, 1.25) (2.5, 2.5, 3.75)	(2.0, 2.5, 1.25) (3.0, 2.5, 3.75)
Mesh size	$40(x) \times 40(y) \times 50(z)$	$40(x) \times 40(y) \times 50(z)$
Mesh interval (Δx)	0.125 cm	0.125 cm
Mesh interval (Δy)	0.125 cm	0.125 cm
Mesh interval (Δz)	0.1 cm	0.1 cm
Time interval (Δt)	2×10^{-5} s	2×10^{-5} s

In the two-dimensional case, calculations are two-dimensional analyses of collisions with various collision angles. Figures 9 and 10 show the computational results with collision angles of 90° and 45°. Conditions in these calculations are shown in Table 4.

4.4 Three-Dimensional Collision of Droplets

Figures 11 and 12 show how two identical fluid spheres collide and merge with each other. All figures are drawn as a wire frame by removing hidden surfaces. Figure 11 shows a head-on collision. After the collision, an asymmetrical frill appears and expands. It is suspected that this expansion is unstable and numerical error causes this instability. In the case of Fig. 12, the direction of the velocity vector is not parallel to the line which passes through the centers of the spheres and merged spheres rotate around each other after collision. The effect of surface tension rounds off the projecting parts of the fluid after the collision. Conditions used in this calculation are shown in Table 5.

V. CONCLUSION

Improvement and extension of the MAC method was attempted and axisymmetrical, two-dimensional and three-dimensional cases of fluid motions with free surfaces were calculated numerically. In this type of calculation, saving memory and computational time is an important problem. This problem is solved by putting markers only sparsely in surface cells and rearranging them at each time step. In addition, a statistical method is used in order to calculate the effect of surface tension in the three-dimensional case, saving computational time and making even three-dimensional calculations easier. Numerical results proposed in this paper are reasonable and they agree with actual observations.

REFERENCES

1) Harlow, F.H. and Welch, J.E., Numerical calculation of time-dependent viscous incompressible flow of fluid with free surface. *Phys. Fluids.*, Vol. **8** (1965), pp. 2182–2189.
2) Katano, Y., Kawamura, T., and Takami, H., Numerical study of drop formation from a capillary jet using a general coordinate system. *Theoretical and Applied Mechanics*, Vol. **34** (Univ. Tokyo Press, 1986), pp. 3–14.
3) Macklin, W.C. and Hobbs, P.V., Surface phenomena and the splashing of drops on shallow liquids. *Science*, Vol. **166** (1969), pp. 107–108.
4) Amsden, A.A. and Harlow, F.H., The SMAC method: A numerical technique for calculating incompressible fluid flow. *Los Alamos Scientific Laboratory Report*, **LA 4370** (1970).